Volume 53
Number 16
28 April 2024
Pages 6841-7242

Dalton Transactions

An international journal of inorganic chemistry

rsc.li/dalton

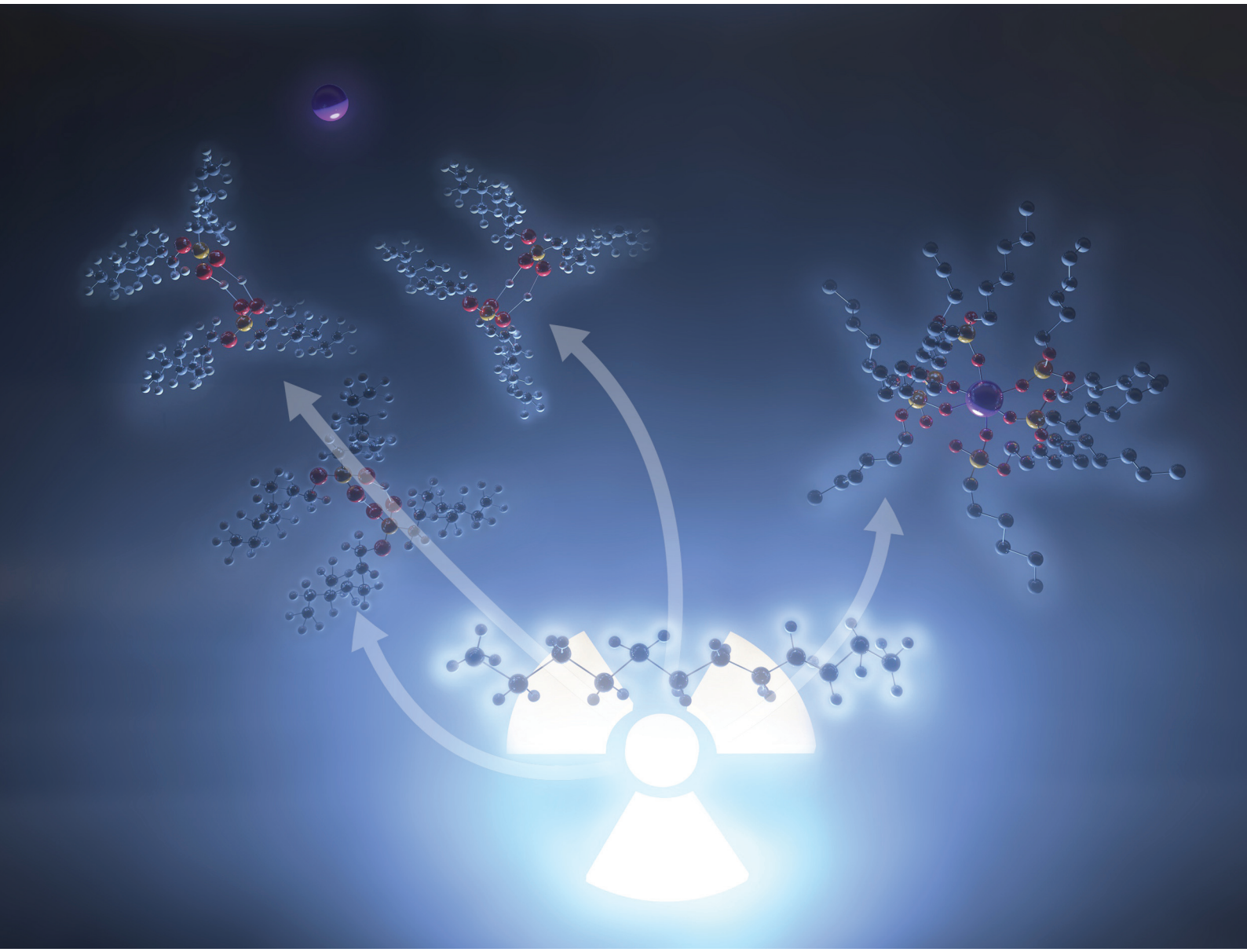

ISSN 1477-9226

ROYAL SOCIETY OF CHEMISTRY

PAPER

Gregory P. Horne *et al.*

Effect of *f*-element complexation on the radiolysis of 2-ethylhexylphosphonic acid mono-2-ethylhexyl ester (HEH[EHP])

Dalton Transactions

ROYAL SOCIETY OF CHEMISTRY

PAPER

View Article Online
View Journal | View Issue

Cite this: *Dalton Trans.*, 2024, **53**, 6881

Effect of *f*-element complexation on the radiolysis of 2-ethylhexylphosphonic acid mono-2-ethylhexyl ester (HEH[EHP])†

Stephen P. Mezyk, *[a] Makayla Baxter,[b,c] Cristian Celis-Barros,[d] Travis S. Grimes,[c] Peter R. Zalupski,[c] Cathy Rae,[c] Christopher A. Zarzana,[c] Andrew R. Cook[e] and Gregory P. Horne *[c]

A systematic study of the impact on the chemical reactivity of the oxidising *n*-dodecane radical cation ($RH^{\bullet+}$) with *f*-element complexed 2-ethylhexylphosphonic acid mono-2-ethylhexyl ester (HEH[EHP]) has been undertaken utilizing time-resolved electron pulse radiolysis/transient absorption spectroscopy and high-level quantum mechanical calculations. Lanthanide ion complexed species, $[Ln((HEH[EHP])_2)_3]$, exhibited vastly increased reactivity (over 10× faster) in comparison to the non-complexed ligand in *n*-dodecane solvent, whose rate coefficient was $k = (4.66 \pm 0.22) \times 10^9$ M^{-1} s^{-1}. Similar reactivity enhancement was also observed for the corresponding americium ion complex, $k = (5.58 \pm 0.30) \times 10^{10}$ M^{-1} s^{-1}. The vastly increased reactivity of these *f*-element complexes was not due to simple increased diffusion-control of these reactions; rather, enhanced hole transfer mechanisms for the complexes were calculated to become energetically more favourable. Interestingly, the observed reactivity trend with lanthanide ion size was not linear; instead, the rate coefficients showed an initial increase (Lu to Yb) followed by a decrease (Tm to Ho), followed by another increase (Dy to La). This behaviour was excellently predicted by the calculated reaction volumes of these complexes. Complementary cobalt-60 gamma irradiations for select lanthanide complexes demonstrated that the measured kinetic differences translated to increased ligand degradation at steady-state timescales, affording ~38% increase in ligand loss of a 1 : 1 $[La((HEH[EHP])_2)_3]$: HEH[EHP] ratio system.

Received 14th February 2024,
Accepted 20th February 2024

DOI: 10.1039/d4dt00424h

rsc.li/dalton

Introduction

For nuclear power to be a sustainable, environmentally-friendly, energy source, research into reprocessing nuclear waste is necessary to close the fuel cycle. Reprocessing minimizes the dangers of stored nuclear waste and recovers valuable elements for future use.[1] The Plutonium Uranium Reduction Extraction (PUREX) process[2] is one approach that has been in use for decades, cleanly co-extracting and subsequently separating uranium and plutonium from nuclear waste. Following this initial separation, a lanthanide (Ln) and minor actinide (MA: americium and curium) rich aqueous phase remains, which can be further treated to reduce the volume and radiotoxicity of nuclear waste for final disposal.[3] However, separating these residual *f*-elements is difficult due to the prevalence and comparable chemical reactivity of their trivalent oxidation states.[4]

To date, dozens of solvent-extraction based processes have been proposed and tested to achieve an efficient Ln/MA separation.[5] Most of these trialled processes involve the use of designer ligands to selectively complex the MAs in either the aqueous or organic phases employed, capitalizing on the greater radial extension and covalent character of the MA 5*f*-orbitals to afford increased thermodynamic stability of the resulting complexes.[6–8]

One of the more recent solvent-extraction based systems proposed for the Ln/MA separation is the Actinide-Lanthanide SEParation Process (ALSEP),[9] which coextracts the trivalent Ln and MA from an aqueous nitric acid phase into an organic phase using a combination of extractants. The most effective ALSEP system utilizes 2-ethylhexylphosphonic acid mono-2-ethylhexyl ester (HEH[EHP], Fig. 1) combined with either *N*,*N*,*N*′,*N*′-tetra(2-ethylhexyl)diglycolamide (TEHDGA) or *N*,*N*,*N*′,*N*′-

[a]*Department of Chemistry and Biochemistry, California State University Long Beach, Long Beach, CA 90804, USA. E-mail: Stephen.mezyk@csulb.edu*
[b]*Department of Chemistry, Northwestern University, Evanston, Illinois 60208, United States*
[c]*Center for Radiation Chemistry Research, Idaho National Laboratory, Idaho Falls, IDP.O. Box 1625, 83415, USA. E-mail: gregory.p.holmbeck@inl.gov*
[d]*Department of Chemistry, Oak Ridge National Laboratory, Oak Ridge, TN, 37830, USA*
[e]*Department of Chemistry, Brookhaven National Laboratory, Upton, New York, 11973, USA*

† Electronic supplementary information (ESI) available. See DOI: https://doi.org/10.1039/d4dt00424h

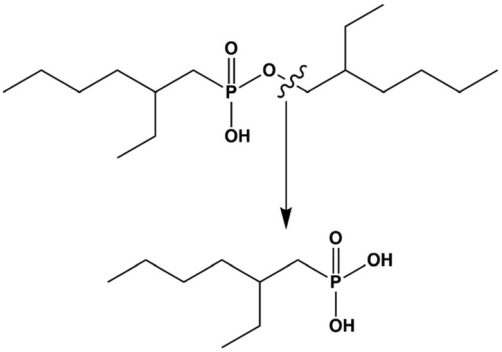

Fig. 1 Structures of 2-ethylhexylphosphonic acid mono-2-ethylhexyl ester (HEH[EHP]) and its major radiation-induced degradation product 2-ethylhexyl phosphonic (HEHP).

tetraoctyl-diglycolamide (TODGA). Following co-extraction, the MA are then selectively transferred back to an acidic aqueous phase by using a polyaminopolycarboxylic acid such as diethylene-triaminepentaacetic acid (DTPA) or hydroxyethylethylenediaminetriacetic acid (HEDTA). The interactions of these ligands with various process relevant metal ions have been extensively examined by previous works to maximize the success of the desired partitioning and stripping processes.[9–11]

That said, there are still significant knowledge gaps in the radiolytic behaviour of ALSEP formulations that must be addressed to fully optimize this technology.[12] All nuclear waste reprocessing systems occur in an intense radioactive environment. The presence of these intense fields (up to kGy h^{-1})[13] of alpha, beta, and gamma radiation can significantly affect the performance of solvent system separations. Moreover, for systems like ALSEP that contain high (~0.75 M) ligand concentrations,[9] radiation effects will be partitioned into direct and indirect pathways. Direct effects involve the direct deposition of ionizing energy into a molecule,[14] which under envisioned ALSEP conditions (*ca.* 25% for 0.75 M HEH[EHP] in *n*-dodecane, a prototypical bench-scale organic solvent) will result in: (i) direct HEH[EHP] ligand (L) fragment species such as radical cations ($L^{\bullet+}$) and free electrons (e^-) by ligand ionization and electronic excitation (L*) followed by bond breakage to give radicals ($L^\bullet$) and molecular degradation products such as 2-ethylhexyl phosphonic (HEHP, Fig. 1):

$$L \rightsquigarrow L^{\bullet+}, e^-, L^*, L^\bullet \rightarrow \text{HEHP} + \text{other products.} \quad (1)$$

The larger fraction of radiation energy is absorbed by the solvent (RH, *e.g.*, *n*-dodecane), resulting in a suite of solvent decomposition products which can react with the added ligand leading ultimately to its destruction:[15–21]

$$RH \rightsquigarrow e^-, H^\bullet, RH^{\bullet+}, R^\bullet, \quad (2)$$

$$\text{Ligand} + RH^{\bullet+} \rightarrow \left[\text{Ligand}^{\bullet+}/\text{Ligand}(+H^+)\right]^+ + RH/R^\bullet, \quad (3)$$

so-called, indirect radiolytic effects. Multiple studies of the radiation-induced degradation chemistry of ligands such as TODGA have been reported for both single and biphasic solvent systems.[17,22–38] The focus of most of these studies was on the radiation-induced degradation of the non-complexed ligand, *i.e.*, in the absence of metal ions. Even under these simplified, and arguably non-representative process conditions, complex radiolytic behaviour was often observed. For example, previous work on an advanced Trivalent Actinide Lanthanide Separation with Phosphorus-Reagent Extraction from Aqueous Komplexes (TALSPEAK) formulation investigated the effects of gamma radiation on the distribution ratios of Lns and MAs and the concentrations of the HEH[EHP] and HEDTA extractants employed.[39] A linear decline was observed for the concentration of HEH[EHP] with increasing gamma dose. Analogous experiments were also performed for ALSEP conditions using HEH[EHP] and TEHDGA as extractants. Again, the concentration of HEH[EHP] decreased linearly with increasing gamma dose, while the concentration of TEHDGA decreased exponentially, as typically observed.[40] In both instances, the formation of HEHP, the major radiation-induced degradation product and common impurity of HEH[EHP], was seen to have a significant and unfavourable impact on the separation of americium and europium.[39,40]

In addition to these works, there is considerable literature reporting very different behaviour for the radiolytic degradation of ligands when complexed to metal ions.[15,16,38,41–47] Kinetic measurements provide major insights into the impacts of metal ion complexation on the chemical reactivity of ligands in radiation environments. Specifically, recent kinetic studies on the reaction of the *n*-dodecane radical cation ($RH^{\bullet+}$) with Ln-complexed TODGA[38] showed that complexation increased chemical reactivity (up to 9.3× faster) and that the $[Ln(TODGA)_3(NO_3)_3]$ complexes had reaction rates that *decreased* as the Ln series was traversed from Nd(III) to Gd(III) to Yb(III). Although these observations are indicative of reaction mechanism changes upon ligand complexation they did not equate to more extensive TODGA radiolysis at steady-state timescales, as reported by Kimberlin *et al.*[48] In contrast, these workers found that americium and europium complexed TODGA afforded a *decreased* rate of radiolysis and a change in the suite and distribution of ligand degradation products. Density Functional Theory Average Local Ionization Energy (DFT-ALIE) calculations further showed that the most likely reaction site was the O-atoms of the coordinated nitrate counter anions rather than the complexed TODGA ligands.[38]

Overall, while metal ion complexation provides additional complications to understanding and predicting the radiolytic behaviour of a reprocessing solvent system, this critical level of insight is not available for HEH[EHP], despite its prevalence in several proposed Ln/MA separation process formulations. Here we present a systematic investigation into the coupled effects of radiation and *f*-element complexation of multiple Ln ions, and one representative MA, americium, on this ligand in *n*-dodecane media. A combination of time-resolved electron pulse and steady-state cobalt-60 gamma irradiations complemented by state-of-the-art DFT calculations were used to evaluate the fundamental mechanisms underpinning HEH[EHP] radiolysis in the presence of metal ions.

Experimental

Caution! The americium-243 solutions used in this work were highly radioactive. Handling was performed in dedicated radiological and nuclear facilities using well established radiological safety protocols.

Materials

Americium-243 (^{243}Am, $\tau_{1/2}$ = 7370 years, E_α = 5.44 MeV) was sourced from on-hand oxide stock ($^{243}Am_2O_3$) at Idaho National Laboratory (INL). This material was purified and characterized as previously described.[49]

HEH[EHP] (98%) was sourced from Marshallton Research Laboratories Inc. (Tobaccoville, NC, USA). Dichloromethane (DCM, ≥99.8%), hydrochloric acid (37% HCl, ≥99.999% trace metals basis), lanthanum(III) nitrate hexahydrate (99.99%), *n*-dodecane (≥99% anhydrous), nitric acid (HNO_3, ≥99.999% trace metals basis), perchloric acid ($HClO_4$, ≥99.999% trace metals basis), piperazine-*N*,*N*′-bis(3-propanesulfonic acid) (PIPPS, ≥97% dry basis), and potassium thiocyanate (KSCN, ≥99.0% ACS Reagent Grade) were obtained from MilliporeSigma (Burlington, MA, USA). Cerium(III) nitrate hexahydrate (99.5%), dysprosium(III) nitrate pentahydrate (99.9%), erbium(III) nitrate hydrate (99.9%), europium(III) nitrate hexahydrate (99.9%), gadolinium(III) nitrate hexahydrate (99.9%), holmium(III) nitrate pentahydrate (99.9%), lutetium(III) nitrate hydrate (99.9%), neodymium(III) nitrate hydrate (99.99%), praseodymium(III) nitrate hydrate (99.9%), samarium(III) nitrate hexahydrate (99.9%), terbium(III) nitrate hydrate (99.9%), and ytterbium(III) nitrate hydrate (99.9%) were supplied by Alfa Aesar (Wardhill, MA, USA). Thulium(III) nitrate hydrate (99.99%) was procured from Thermo Scientific Chemicals (Waltham, MA, USA). The 2% OPTIMA HNO_3 solutions were from PerkinElmer. Standard lanthanide nitrate solutions were sourced from Inorganic Ventures CMS-1 (Christiansburg, VA, USA), ICP-MS instrument calibrations used SPEX (Cole-Palmer, Vernon Hills, IL, USA) CertifPrep CL-CAL-2 ICP-MS standards, with an internal standard sample of 20 ppb rhodium from SPEX CertifPrep PLRH2-2Y. Solvents used for measurements using liquid chromatography/mass spectrometry (water with 0.1% formic acid, acetonitrile with 0.1% formic acid, and 2-propanol) were all MilliporeSigma hypergrade for LC-MS LiChrosolv®. Di(2-ethylhexyl)phosphoric acid (HDEHP) used as internal standard was sourced from Sigma-Aldrich (now MilliporeSigma). Nitric acid used for inductively-couples plasma/mass spectrometry measurements was Fisher (Hampton, NH, USA) Optma™, for Ultra Trace Elemental Analysis. All commercial chemicals were used without further purification. Ultra-pure water (18.2 MΩ) was used in the preparation of all aqueous solutions.

Irradiations

Time-resolved electron pulse irradiation. Kinetics for the reaction of the $RH^{\bullet+}$ radical cation with HEH[EHP] and its *f*-element complexes, [Ln/Am((HEH[EHP])$_2$)$_3$], were measured at 800 nm over 200 ns using the picosecond electron pulse radiolysis/transient absorption system at the Brookhaven National Laboratory (BNL) Laser Electron Accelerator Facility (LEAF). The LEAF detection system has been previously described.[50] Dosimetry was performed using N_2O saturated solutions of 10 mM KSCN at λ_{max} = 470 nm (assuming $G \times \varepsilon = 5.2 \times 10^{-4}$ m^2 J^{-1}).[51]

Samples comprised of varying concentrations of HEH[EHP] dissolved in 0.5 M DCM/*n*-dodecane solution in the presence and absence of its Ln/Am complexes. For the Ln-containing samples, a HEH[EHP]/0.5 M DCM/*n*-dodecane stock solution was contacted in a 1 : 1 volume ratio with an aqueous solution of 50 mM PIPPS (pH 4) and ~2.5 mM lanthanide nitrate. The presence of PIPPS in the aqueous phase minimized pH migration due to the release of H_{aq}^+ by the HEH[EHP] ion exchanger. These biphasic systems were shaken for 5 min and then allowed to settle (phase separate) overnight. The metal ion loaded organic phases were then removed for irradiation, while the aqueous phases were retained for subsequent elemental analysis, see below. The preparation of the americium-containing samples was like that followed for the lanthanides, except that 1 mM ^{243}Am was present during liquid–liquid equilibration. The extraction conditions ensured a quantitative extraction of americium by HEH[EHP]. After extraction the americium-containing organic phase was diluted using 0.5 M DCM/*n*-dodecane. A series of samples prepared for irradiation studies contained 1.0, 0.75, 0.50, and 0.25 mM ^{243}Am. Sample solutions were irradiated in 1.00 cm optical pathlength, screw-cap sealed, Suprasil (Starna Scientific Ltd, Ilford, United Kingdom) cuvettes.

The measured $RH^{\bullet+}$ radical cation decays were fitted using a double-exponential decay function:

$$k_{obs} = A_1 \exp(-k_1 t) + A_2 \exp(-k_2 t) + B, \quad (4)$$

starting at 2 ns after the electron pulse to allow for the instrument response, where k_{obs} was the overall rate of decay for the absorbance at 800 nm, A_i are the optical density amplitudes, k_i are the pseudo-first-order rate coefficients (s^{-1}), t is time (s), and B is a baseline offset correction. The faster exponential decay (A_1 and k_1 parameters in eqn (4)) corresponds to the total reaction of the $RH^{\bullet+}$ radical cation with both the remaining fraction of non-complexed HEH[EHP] ligand and the [Ln/Am((HEH[EHP])$_2$)$_3$] complex.[52] Subtraction of the non-complexed ligand reactivity from the total fitted pseudo-first-order k_1 values, and plotting the difference against the complex concentration, gave the desired second-order rate coefficients for only the $RH^{\bullet+}$ radical cation reaction with the complex. The second exponential decay (A_2 and k_2 parameters in eqn (4)) and B variables account for the slower tailing absorption decrease usually seen in these systems at this wavelength.[18] The overall quoted rate coefficient errors (1σ) are a quantitative combination of measurement precision (~4%) and sample concentration (initial concentration (~5–9%) and dilution (<1%)) errors.

Steady-state gamma irradiations. The effect of *f*-element complexation on the steady-state degradation of HEH[EHP]

was studied using the INL Center for Radiation Chemistry Research's Nordion GammaCell 220E and Foss Therapy Services Model 812 cobalt-60 irradiators. The organic phase of different HEH[EHP] solution permutations were irradiated using either 30 mM or 0.75 M HEH[EHP]: (i) HEH[EHP]/*n*-dodecane (organic-only); (ii) HEH[EHP]/*n*-dodecane pre-equilibrated (1 : 1 organic : aqueous phase ratio) with 0.2 M aqueous PIPPS/0.4 mM HNO_3 solution; and (iii) HEH[EHP]/*n*-dodecane loaded with either 18 mM Eu(III) or 2.5 mM La(III) following pre-equilibration with 0.2 M aqueous PIPPS/0.4 mM HNO_3 solution. Each single-phase organic solution permutation was irradiated in triplicate to doses up to 2 MGy. Samples comprised of 2–4 mL of solution sealed in 20 mL screw-cap scintillation vials. Despite the original air headspace, samples were considered 'deaerated' due to the radiolytic consumption of dissolved oxygen at relatively low absorbed gamma doses. Fricke dosimetry[53] was previously used to establish the dose rate for each irradiator's sample configuration and radiation field. Dose rates were corrected for the radioactive decay of cobalt-60 ($\tau_{1/2}$ = 5.27 years) and the electron density of HEH[EHP]/*n*-dodecane solution permutations *vs.* water.[14] Radiation chemical yields (*G*-values, μmol J^{-1}) and dose constants (*d*-values, kGy^{-1}) were calculated where appropriate.

Analysis

Gas chromatography flame ionization detection (GC-FID). Quantification of HEH[EHP] by GC-FID was achieved using an Agilent (Santa Clara, CA, USA) 7890 gas chromatographs, equipped with an Agilent 7693 autosampler and a flame ionization detector. A five-point calibration curve and an additional blank were employed. HDEHP was used as an internal standard and added to the calibration standards and samples at a constant concentration. Samples were diluted in 2-propanol by a factor of approximately 10^6 compared to their analytical concentrations. Quality control standards (QCs) at mid and high points on the calibration curve were injected every 10 samples to ensure the continued validity of the calibration curve. All calibration samples, QCs, and samples were injected 5 times.

Inductively-coupled plasma mass spectrometry (ICP-MS). The exact concentrations of lanthanide ion extracted into the organic phases of each system was determined by ICP-MS. Pre- and post-contact lanthanide nitrate-containing aqueous samples were digested entirely in 2% Optima™ grade HNO_3 and diluted, typically 100–500×. Samples were run on an Agilent 7500ce ICP-MS using a helium reaction cell to reduce isobaric interferences. All standard lanthanide nitrate solutions, instrument calibration standards, and the internal Rh standard were run at the beginning and end of each sample set measurement. Confirmation of these extracted concentrations was achieved by measuring the organic phase solutions by the same approach. The same concentration values were obtained; however, the organic measurements had much larger reproducibility errors (~25%).

Gamma spectroscopy. The distribution of ^{243}Am was quantified by gamma spectroscopy using an ORTEC GEM50P4 coaxial HPGe detector and DSPEC gamma spectrometer. After americium extraction, aliquots of the aqueous and organic liquid phases (diluted 100-fold with *n*-dodecane) and the ^{243}Am activity monitored using its characteristic 74.66 keV gamma ray emission.

Computations

Structure calculations. To investigate the differences in structure and bonding on the $[Ln((HEH[EHP])_2)_3]$ complexes, a working model had to be assumed based on our current knowledge of lanthanide ion coordination and HEH[EHP]. The coordination numbers of lanthanide complexes are most commonly 8–9, although can be as high as 12 due to their large size and largely ionic character of their bonds.[54] In *n*-dodecane HEH[EHP] exists predominantly as a dimer[55] linked by a pair of hydrogen bonds between the two phosphate moieties. This arrangement significantly reduces the number of possible conformations by which HEH[EHP] can bind to lanthanide ions. Based on these considerations, geometry optimizations were performed for models of the $[Ln((HEH[EHP])_2)_3]$ (Ln = La, Ce, Nd, Gd, Ho, Yb, and Lu) complexes by trimming the ethyl groups on the hexyl hydrocarbon chains (ESI, Fig. S1†). These optimizations were performed using scalar relativistic (ZORA) DFT. The generalized gradient approximation (GGA) functional PBE was used along with the STO-TZP basis set as implemented in ADF2020.[56,57] Frequency calculations confirmed that the structures were in local minima.

The interaction between the lanthanide ion centres and the HEH[EHP] dimers was further studied by the Bader's quantum theory of atoms in molecules (QTAIM).[58,59] The molecular density necessary to obtain QTAIM metrics was obtained from Kohn–Sham-DFT calculations performed in ORCA[60,61] using the hybrid GGA PBE0 functional along with the DKH-def2-TZVP basis set for all atoms except the lanthanide ions, which were treated with the SARC-TZVP basis set. Scalar relativistic effects were included using the second-order relativistic Hamiltonian DKH after which the AIMALL package was used to calculate the QTAIM metrics.[62] It is important to note that the molecular density lacks static correlation, and therefore an overestimation of the bonding interactions may be expected in the QTAIM metrics. Such corrections should be included using multiconfigurational wave functions, but in our case were impractical due to the size of the system (256 atoms). Regardless, trends across the series did not change significantly when these effects are not included as shown previously.[63]

Among the variety of metrics provided by QTAIM calculations, herein we focused on topological volumes. Given the natural partition of the molecular electron density in this formalism, atomic fragments (basins) are well defined, and volumes can be estimated. This allows for comparisons between molecular volumes and individual metal ion volumes.

Thermodynamic calculations. Electronic structure calculations on the HEH[EHP] ligand and its lanthanide ion complexes were completed with the Gaussian16, rev. B.01[64] and Gaussview 6.1.1[65] programs, using the B3LYP functional, 6-

31+G* basis set, and the polarizable continuum model for the *n*-dodecane solvent. Optimal geometries were confirmed to be local minima using frequency calculations, and multiple starting points were used in some cases to find the lowest energy structures. Reaction free energies (ΔG) were computed with corrections for standard states and the solvent as a reactant as outlined by Kelly *et al.*[66,67]

Results and discussion

^{60}Co degradation rate measurements

The change in concentration of HEH[EHP] as a function of absorbed gamma dose is shown Fig. 2(A) and (B) for a variety of solution formulation conditions. In Fig. 2(A), all solutions contained 0.75 M HEH[EHP], which is representative of the concentration envisioned for the ALSEP process.[9] In addition to the organic-only data measured by this work, results from biphasic solvent test loop irradiations[40] for a range of contacted HNO_3 concentrations (2.0, 3.0, and 4.0 M) are plotted alongside. Under these high HEH[EHP] concentration regimes the rate of HEH[EHP] radiolysis was essentially independent of solution formulation, as all presented permutations exhibited a linear decay with absorbed gamma dose, affording an average radiolytic yield of $G = -0.14 \pm 0.04$ μmol J^{-1}. This consistent value highlights the significant radiation robustness of HEH[EHP] compared with other contemporary MA/Ln separation ligands. For example, octylphenyl-*N*,*N*-diisobutylcarbamoylmethyl phosphine oxide (CMPO) was found to have a degradation rate of $G = -0.18$ μmol J^{-1}.[68] As noted previously for the gamma and alpha radiolysis of CMPO,[68–70] the investigated 0.75 M HEH[EHP] systems exhibited zero-order kinetics, *i.e.*, the rate of loss of HEH[EHP] was independent of ligand concentration. This behaviour is atypical, as most other MA/Ln separation ligands, such as TODGA, decay exponentially with absorbed radiation dose, with their radiolytic behaviour described using *d*-values, *e.g.*, *d*(TODGA) = 5.7×10^{-3} kGy^{-1}, for organic-only conditions.[71,72]

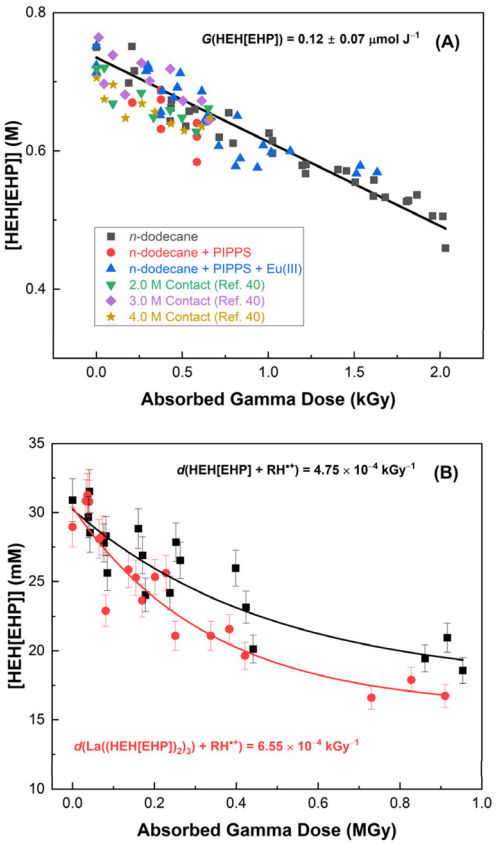

Fig. 2 (A) Concentration of HEH[EHP] as a function of absorbed dose from the gamma irradiation of 0.75 M HEH[EHP] under: organic-only (■); pre-equilibrated with PIPPS/HNO_3 solution (●); and contacted with 18 mM Eu(III) from PIPPS/HNO_3 solution (▲) conditions. Data sets for 0.75 M HEH[EHP]/*n*-dodecane in contact with 2.0 (▼), 3.0 (◆), and 4.0 (★) M HNO_3 solutions are from ref. 40. (B) Concentration of HEH[EHP] as a function of absorbed dose from the gamma irradiation of 30 mM HEH[EHP] under organic-only (■) and contacted with 2.5 mM La(III) from PIPPS/HNO_3 solution (●) conditions. Dose constants (*d*-values) were calculated from initial-dose linear fits of Ln([La((HEH[EHP])$_2$)$_3$]) *vs.* absorbed gamma dose.

The apparent absence of any significant solvent system effects (*i.e.*, HNO_3 contact and/or metal ion complexation) on the rate of 0.75 M HEH[EHP] degradation by gamma radiolysis shown in Fig. 2(A) is also interesting, as other extraction ligands exhibit such a dependence. For example, the *G*- and *d*-values reported for CMPO and TODGA, respectively, decreased when irradiated in contact with HNO_3 *vs.* organic-only.[72,73] Moreover, complexation of Eu(III) and Am(III) ions by TODGA has been shown to decrease the rate of TODGA radiolysis.[48] The absence of solvent system effects for these HEH[EHP] irradiations is likely a consequence of its high concentration: (i) outcompeting other potential organic phase solutes (*e.g.*, H_2O and HNO_3) for the primary products of solvent radiolysis, thereby inhibiting any potential radioprotective effects; and (ii) masking any changes in radiolytic behaviour associated with the relatively lower concentration (~18 mM) of [Eu((HEH[EHP])$_2$)$_3$] complexes present in our system.

To further investigate the latter effect, a much lower concentration (30 mM) of HEH[EHP] was used in conjunction with La(III) (2.5 mM) to increase the ratio of [La((HEH[EHP])$_2$)$_3$] : HEH[EHP] to 1 : 1 *vs.* 1 : 36 in the 0.75 M HEH[EHP] solvent systems, the results for which are shown in Fig. 2(B). For both non-complexed HEH[EHP] and [La((HEH[EHP])$_2$)$_3$], the measured concentration of HEH[EHP] now decreases exponentially, not linearly, with absorbed gamma dose, affording dose coefficients of *d*(HEH[EHP]) = 4.75×10^{-4} kGy^{-1} and *d*([La((HEH[EHP])$_2$)$_3$]) = 6.55×10^{-4} kGy^{-1} for organic-only conditions. Both of these 30 mM HEH[EHP] *d*-values are lower than those for complementary CMPO and TODGA solvent systems,[72,73] once again demonstrating the significant radiation robustness of HEH[EHP]. Interestingly, the higher fraction of [La((HEH[EHP])$_2$)$_3$] : HEH[EHP] showed a significant increase (~38%) in the associated dose coefficient relative to the non-complexed HEH[EHP] system, indicating that metal ion complexation increases the susceptibility of HEH[EHP] to

radiolytic damage. We attribute this increase to the much faster reactivity of the [La(HEH[EHP]$_2$)$_3$] complex with the RH$^{\bullet+}$ radical cation, see the following reaction kinetics discussion. The enhanced reactivity incurred through complexation will have significant implications for all proposed UNF reprocessing schemes, especially those intent on achieving higher metal ion loading.

Reaction kinetics

As shown in eqns (2) and (3), the electron pulse radiolysis of *n*-dodecane produces multiple reactive species that can react with HEH[EHP] and its metal ion complexes. For lower concentrations (<30 mM) of HEH[EHP], the RH$^{\bullet+}$ radical cation is the dominant reacting species, as the initially formed electronically excited states are typically very short-lived (~2–4 ns),[74] and the solvated electrons (e_s^-) and radical species (H$^\bullet$ and R$^\bullet$) produced are expected to react with dissolved oxygen (O_2) to give the relatively non-reactive superoxide ($O_2^{\bullet-}$) and peroxyl radicals ($HO_2^\bullet$):[14]

$$e_s^- + O_2 \rightarrow O_2^{\bullet-}, \quad (5)$$

$$H^\bullet + O_2 \rightarrow HO_2^\bullet \rightleftharpoons H_{aq}^+ + O_2^{\bullet-}, \quad (6)$$

$$R^\bullet + O_2 \rightarrow RO_2^\bullet. \quad (7)$$

These reactions isolate the RH$^{\bullet+}$ radical cation in these systems, which has been previously shown to exhibit significant reactivity with UNF reprocessing ligands:[16–21,32,38,72,73,75,76]

$$\text{Ligand} + RH^{\bullet+} \rightarrow \text{products}. \quad (8)$$

Moreover, it is important to note that at the ligand concentrations used in these kinetic studies (7.5–30 mM), HEH[EHP] will dimerize in *n*-dodecane to reduce the repulsion of the polar phosphate group in the non-polar media, producing dimer species as shown in Fig. 3. Kimberlin and Nash reported the HEH[EHP] dimer association constant (K) in *n*-dodecane as K = 5500.[55] For the HEH[EHP] concentrations used in these kinetic studies, the dimer fraction ranges from 86–93%, while for the HEH(EHP) concentrations used in the above steady-state gamma irradiations, over 96% would be dimerized. As we have a mix of monomer and dimer HEH[EHP] species under

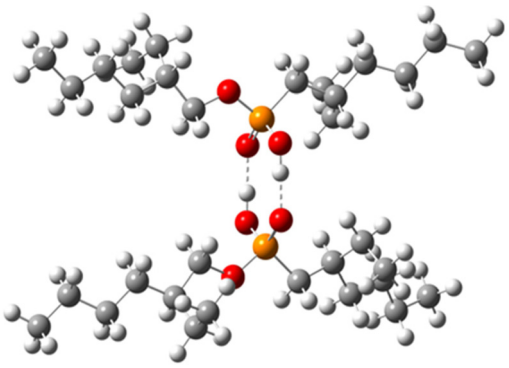

Fig. 3 Model structure for the HEH[EHP] dimer.

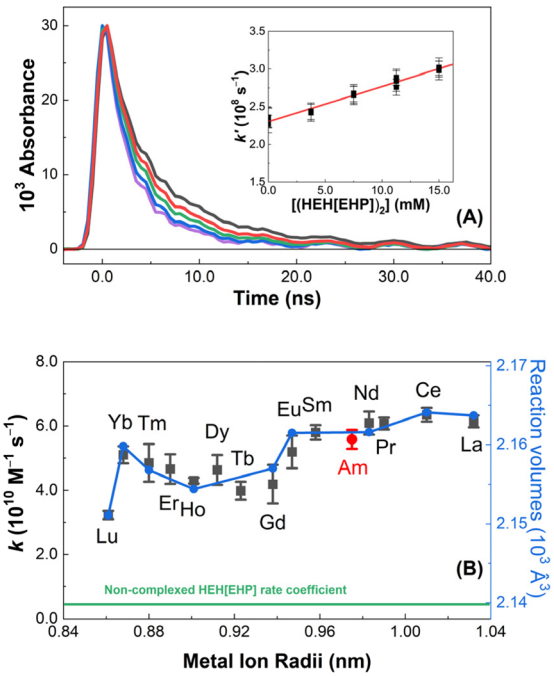

Fig. 4 (A) Transient absorption RH$^{\bullet+}$ radical cation decay kinetics in *n*-dodecane solution containing 0.50 M CH_2Cl_2 at 25 °C containing zero (black), 7.5 (red), 15.0 (green), 22.5 (blue), and 30.0 (purple) mM HEH[EHP]. Inset: Second-order kinetic rate coefficient determination for this reaction, solid line is weighted linear fit corresponding to a value of (4.66 ± 0.22) × 10^9 M^{-1} s^{-1}, R^2 = 0.976. (B) Second-order rate coefficients determined for Ln((HEH[EHP])$_2$)$_3$ and Am((HEH[EHP])$_2$)$_3$ in *n*-dodecane. Solid blue line is reactivity prediction based upon DFT volume calculations, normalized at Lu(III) and Ce(III) to experimental data. Horizontal green line shows rate coefficient for only HEH[EHP].

our experimental conditions we have determined its reactivity with the RH$^{\bullet+}$ radical cation for the dimer species (see Fig. 4A, inset), affording a second-order rate coefficient of k = (4.66 ± 0.22) × 10^9 M^{-1} s^{-1}. This value is shown in comparison to the metal–ligand complex values in Fig. 4B. The non-complexed HEH[EHP] dimer's reactivity with the RH$^{\bullet+}$ radical cation is effectively diffusion-controlled, as based on a simple, diffusion-controlled, Smoluchowski equation calculation:[77]

$$k_{diff} = 4\pi(D_{RH^{\bullet+}} + D_X)(r_{RH^{\bullet+}} + r_X). \quad (9)$$

While neither the HEH[EHP] dimer or RH radical cations are spherical, for this estimation of the impact of size on rate we can assume both reactant sizes may be approximated as such. The flexible, saturated carbon chains of both molecules will explore a wide range of configurations making various molecular shapes and sizes, supporting this simplification. In eqn (9), the equation parameters for the RH$^{\bullet+}$ radical cation are set equal to those of *n*-dodecane, with a self-diffusion coefficient (D) of 8.1 × 10^{-11} m^2 s^{-1} and radius (r, taken as $\frac{1}{2}$ its calculated end-to-end length) of 7.3 × 10^{-10} m.[78,79] The radius of the HEH[EHP] dimer is derived from its calculated its reaction volume (see Table 1) where we have assumed a spherical shape for this volume to give r = 3.85 × 10^{-10} m, which corre-

Table 1 Summary of second-order rate coefficients and calculated DFT reaction volume parameters for HEH[EHP] and its [Ln/Am((HEH[EHP])$_2$)$_3$] complexes

Metal	k (10^{10} M^{-1} s^{-1})	Error (10^{10} M^{-1} s^{-1})	Ionic radius (nm)	Reaction volumes (Å^3)	Metal volumes (Å^3)
Non-complexed	0.233	0.011		721.3[a]	
La	6.14	0.18	1.032	2163.7	20.27
Ce	6.35	0.22	1.01	2164.1	19.27
Pr	6.07	0.19	0.99		
Nd	6.09	0.36	0.983	2161.6	17.77
Pm					
Sm	5.80	0.23	0.958		
Eu	5.19	0.51	0.947	2161.5	
Gd	4.19	0.60	0.938	2157.0	15.71
Tb	3.99	0.28	0.923		
Dy	4.63	0.46	0.912		
Ho	4.30	0.09	0.901	2154.4	14.00
Er	4.66	0.46	0.89		
Tm	4.85	0.58	0.88	2156.8	13.53
Yb	5.10	0.27	0.868	2159.8	13.36
Lu	3.23	0.13	0.861	2151.1	12.57
Am	5.58	0.30	0.975		

[a] Calculated value for the HEH[EHP] dimer.

lates to a diffusion value based on the Stokes–Einstein equation of $D = 6.5 \times 10^{-10}$ m^2 s^{-1}.[77] This value is slightly smaller than the corresponding measured value in heptane ($D = 1.01 \times 10^{-9}$ m^2 s^{-1}).[80] Based on these literature data we calculate $k_{diff} = 6.1 \times 10^9$ M^{-1} s^{-1} for eqn (8) for the HEH[EHP] dimer species, which is slightly faster than our measured value, $k = (4.66 \pm 0.22) \times 10^9$ M^{-1} s^{-1}.

Energetically, the computed reaction free energy for the transfer of the hole from the RH$^{\bullet+}$ radical cation to a HEH[EHP] dimer is $\Delta G = -0.12$ eV. Our calculations show that this reaction is accompanied by a substantial reorganization of the dimer species, twisting the central phosphate ring out of plane and moving both hydrogen bonding protons to one side of the dimer. Much of the hole density resides on the alkyl moieties of the HEH[EHP] molecule that donated the proton. This is expected, as it is more difficult to oxidise the phosphate core. An internally proton shifted form of the HEH[EHP] dimer radical cation, where a neighbouring proton from one of the alkyl chains has transferred to one of the oxygens, was computed to be more stable by 0.52 eV. It is likely that other protons in the radical cation can transfer in a similar fashion, albeit at slightly less favourable energies. Despite this more energetically-favourable reaction, this product is unlikely to occur during hole transfer from the RH$^{\bullet+}$ radical cation, as it involves crossing the barrier to break a C–H bond, reasonably resulting in a slower rate. However, such products might be the ultimate result, pointing to a vector for radiolytic damage for the HEH[EHP] molecule.

We also note that the only energetically feasible hole transfer reaction from the RH$^{\bullet+}$ radical cation to the HEH[EHP] monomer involves an internal proton transfer ($\Delta G = -0.71$ eV), possibly making such a process kinetically slow. Proton transfer from the RH$^{\bullet+}$ radical cation to an oxygen atom in HEH[EHP] may also be a competitive reaction ($\Delta G = -0.26$ eV) with a similar C–H bond breaking barrier, resulting in a dodecane neutral radical (R$^{\bullet}$) and a HEH[EHP]H$^+$ species.

Upon metal ion complexation the reaction kinetics rate coefficients increased by over an order of magnitude, see Fig. 4B. All the kinetic data obtained in this study are summarized in Table 1, with the individual second-order rate coefficient plots given in Fig. S2.† In addition to the investigated lanthanide complexes, an americium complex of HEH[EHP] was also measured in this work, [Am(HEH[EHP]$_2$)$_3$]. The reactivity of the RH$^{\bullet+}$ radical cation was seen to be consistent with the measured and predicted lanthanide-complex trends. The absolute rate value for [Am(HEH[EHP]$_2$)$_3$] was found to be very similar to that of the [Nd(HEH[EHP]$_2$)$_3$], which is consistent with Nd(III) typically being used as an Am(III) surrogate in separation studies.[81,82]

The reactions for the RH$^{\bullet+}$ radical cation with the [Ln/Am((HEH[EHP])$_2$)$_3$] complexes are over an order of magnitude faster than for the non-complexed ligand, which is not consistent with the predictions of the slightly enhanced diffusion-controlled reactivity (eqn (9)) based on the increased complex reaction volumes (Table 1) values. In addition, while the kinetic trend observed for the RH$^{\bullet+}$ radical cation's reactivity shows an overall increase with metal ionic radius, as shown in Fig. 4B, this trend it is not the expected linear change based upon only the lanthanide ion contraction giving smaller complexes. There are distinct jumps observed that are not attributable to just measurement errors. As such, additional DFT calculations were performed to gain further insight into this unexpected chemistry. Geometry optimization of selected [Ln((HEH[EHP])$_2$)$_3$] complexes were performed with QTAIM metrics obtained using the AIMALL software.[62] To improve complex geometry and speed up the calculations, the branched hexyl-ethyl chains were substituted by hexyl moieties. Based on literature, we presumed here that the complexes in *n*-dodecane possess a neutral charge, by having one proton of each coordinating HEH[EHP] dimer unit removed to allow complexation to the metal ion.[52,83] Table 1 summarizes the calculated metal ion-centre reaction volumes, where these values are the integration of the electron density up to $\rho(r) = 0.001$ a.u. This same calculation was performed for the HEH[EHP] dimer to give its size in *n*-dodecane, as used in eqn (9).

Based on the correlations between the computed Ln(III) and molecular volumes with their corresponding metal ionic radii we learn that the size of the complex is *not* only correlated with the effective size of the metal in the complex, (see Table 1 and Fig. S3†). Moreover, to compare the metal–ligand calculated volume values to the measured rate coefficients of this study, the former were normalized to the rate coefficients for Lu(III) (lowest) and Ce(III) (highest) complex values. Based upon this empirical normalization, excellent agreement between the experimental rate coefficients and predicted reaction volumes is seen (Fig. 4B), confirming that the changes in the experimental data are real, and to be expected for the different complexes.

If we consider the complexation process, which involves the metal ion taking the place of one of the hydrogen atoms in each

dimer,[83] it allows for further delocalisation of the electron density from the metal ion into the ligand radical cation. This would facilitate electron–hole reactions by reducing some of the reorganization necessary during hole transfer. Furthermore, along with the (relatively) large size of the HEH[EHP] complexes, this delocalisation allows near-diffusion controlled hole transfer to the complexes, at about 10× the rate coefficient measured for non-complexed HEH[EHP] in *n*-dodecane.

Conclusions

A combination of steady-state gamma and transient electron pulse radiolysis experiments have been performed to investigate the enhanced reactivity of trivalent *f*-element complexation of the HEH[EHP] ligand in *n*-dodecane solvent. Gamma irradiations showed enhanced ligand degradation upon lanthanide ion complexation. We attribute these steady-state observations to the enhanced reactivity of the [Ln/Am((HEH[EHP])$_2$)$_3$] complexes to solvent radiolysis products relative to the non-complexed ligand. Specifically, we found that the rates of reaction between the $RH^{\bullet+}$ radical cation and the investigated [Ln/Am((HEH[EHP])$_2$)$_3$] complexes were enhanced by over 10×, and decreased as the lanthanide series was traversed. However, these changes were not smoothly linear, as usually observed for lanthanide-contraction dominated chemistry. Instead, these kinetic changes were in excellent agreement with the predictions of DFT calculated reaction volumes, which accurately predicted these discontinuities.

The presented DFT calculations showed that the relatively large reactivity increases for the [Ln/Am((HEH[EHP])$_2$)$_3$] complexes was not due to only changes in size, relative to the non-complexed HEH[EHP] dimer. Rather, a new $RH^{\bullet+}$ radical cation reaction mechanism is being facilitated, which we attribute to hole transfer to the complex being enhanced by the delocalization of electron density from the coordinated metal ion. Our calculations show that the ligand's phosphate centres, which, when non-complexed, do not react well with the $RH^{\bullet+}$ radical cation, but dramatically increase in reactivity when bonded to the metal ion. This unique interaction facilitates the delocalization of the hole from $RH^{\bullet+}$ radical cation across the metal ion and complexant, thus making the hole transfer more favourable and rapid.

The increased reactivity of the [Ln/Am(HEH[EHP]$_2$)$_3$] complexes is much greater than previously observed for the $RH^{\bullet+}$ radical cations' reactivity with other lanthanide ion complexed ligands, such as TODGA[72] and HONTA,[15] and has implications at steady-state timescales. These observations warrant extensive investigation into the impacts of metal ion complexation on other proposed separation ligands to establish a rule-of-thumb for expected implications on process performance.

Conflicts of interest

There are no conflicts to declare.

Acknowledgements

This research has been funded by the United States Department of Energy (U.S. DOE) Assistant Secretary for Nuclear Energy, under the Material Recovery and Waste Form Development Campaign, DOE-Idaho Operations Office Contract DE-AC07-05ID14517 and DE-NE0008406 Nuclear Energy Universities Program (NEUP) grant. Cook and electron pulse irradiation experiments at LEAF of the BNL Accelerator Centre for Energy Research were supported by the U.S. DOE, Office of Basic Energy Sciences, Division of Chemical Sciences, Geosciences, and Biosciences under contract DE-SC0012704. Baxter was supported by the U.S. DOE, Office of Science, Office of Workforce Development for Teachers and Scientists (WDTS) under the Science Undergraduate Laboratory Internships Program (SULI).

References

1 International Atomic Energy Agency, *Status and trends in spent fuel reprocessing*, IAEA-TECDOC-1467, 2005, pp. 1–108.
2 H. A. C. McKay, *The PUREX process*, ed. W. W. Schulz, K. P. Bender, L. L. Burger and J. D. Navratil, CRC Press, Inc., Baca Raton, FL, 1990, pp. 1–9. ISBN: 0-8493-6389-6.
3 J. Veliscek-Carolan, Separation of actinides from spent nuclear fuel: A review, *J. Hazard. Mater.*, 2016, **318**, 266–281.
4 Y. Fan, Y. Li, X. Shu, R. Wu, S. Chen, Y. Jin, C. Xu, J. Chen, C. Huang and C. Xia, Complexation and separation of trivalent actinides and lanthanides by a novel DGA derived from macrocyclic crown ether: Synthesis, extraction, and spectroscopic and density functional theory studies, *ACS Omega*, 2021, **6**, 2156–2166.
5 E. D. Collins, G. D. Del Cul, B. B. Spencer, R. T. Jubin, C. Maher, I.-T. Kim, H. Lee, Y. S. Fedorov, V. F. Saprykin, V. I. Beznosyuk, A. B. Kolyadin, P. Baron, M. Miguirditchian, C. Sorel, Y. Morita, R. Taylor, A. Khaperskaya, C. Hill, R. Malmbeck, J. Law, G. Angelis, L. Boucher, X. Xeres, E. Mendes, T. Inoue, J. P. Glatz, M. Kormilitsyn, J. Uhlíř, V. Ignatiev, J. Serp and S. Delpech, *State-of-the-art report on the progress of nuclear fuel cycle chemistry*, NEA No. 7267, OECD-NEA, Paris, France, 2018, pp. 1–300.
6 K. A. Pace, V. V. Klepov, A. A. Berseneva and H.-C. zur Loye, Covalency in Actinide Compounds, *Chem. – Eur. J.*, 2021, **27**, 5835–5841.
7 G. R. Choppin, Covalency in f-element bonds, *J. Alloys Compd.*, 2002, **344**, 55–59.
8 N. Kaltsoyannis, Does covalency increase or decrease across the actinide series? Implications for minor actinide partitioning, *Inorg. Chem.*, 2013, **52**, 3407–3413.
9 A. V. Gelis and G. J. Lumetta, Actinide-Lanthanide Separation Process - ALSEP, *Ind. Eng. Chem. Res.*, 2014, **53**, 1624–1631.

10 G. A. Picay, B. D. Etz, S. Vyas and M. P. Jensen, Characterization of the ALSEP process at equilibrium: Speciation and stoichiometry of the extracted complex, *ACS Omega*, 2020, **5**, 8076–8089.
11 G. B. Hall, V. E. Holfeltz, E. L. Campbell, D. Boglaienko, G. J. Lumetta and T. G. Levitskaia, Evolution of acid-dependent Am^{3+} and Eu^{3+} organic coordination environment: Effects on the extraction efficiency, *Inorg. Chem.*, 2020, **59**, 4453–4467.
12 A. T. Ta, M. P. Jensen and S. Vyas, Dynamic and solvation behaviors of ALSEP organic ligands, *J. Phys. Chem. B*, 2019, **123**, 8550–8558.
13 B. J. Mincher, S. P. Mezyk and L. R. Martin, A pulse radiolysis investigation of the reactions of tributyl phosphate with the radical products of aqueous nitric acid irradiation, *J. Phys. Chem. A*, 2008, **112**, 6275–6280.
14 J. W. T. Spinks and R. J. Woods, *An Introduction to Radiation Chemistry*, Wiley-Interscience, New York, 3rd edn, 1990.
15 T. Toigawa, D. R. Peterman, D. S. Meeker, T. S. Grimes, P. R. Zalupski, S. P. Mezyk, A. R. Cook, S. Yamashita, Y. Kumagai, T. Matsumura and G. P. Horne, Radiation-induced effects on the extraction properties of hexa-n-octylnitrilotriacetamide (HONTA) complexes of americium and europium, *Phys. Chem. Chem. Phys.*, 2021, **23**, 1343–1351.
16 C. Celis-Barros, C. D. Pilgrim, A. R. Cook, T. S. Grimes, S. P. Mezyk and G. P. Horne, Influence of uranyl complexation on the reaction kinetics of the dodecane radical cation with used nuclear fuel extraction ligands (TBP, DEHBA, and DEHiBA), *Phys. Chem. Chem. Phys.*, 2021, **23**, 24589–24597.
17 C. A. Zarzana, G. S. Groenewold, B. J. Mincher, S. P. Mezyk, A. Wilden, H. Schmidt, G. Modolo, J. F. Wishart and A. R. Cook, A comparison of the γ-radiolysis of TODGA and T(EH)DGA using UHPLC-ESI-MS analysis, *Solvent Extr. Ion Exch.*, 2015, **33**, 431–447.
18 S. P. Mezyk, B. J. Mincher, S. B. Dhiman, B. Layne and J. F. Wishart, The role of organic solvent radical cations in separations ligand degradation, *J. Radioanal. Nucl. Chem.*, 2016, **307**, 2445–2449.
19 S. P. Mezyk, G. P. Horne, B. J. Mincher, P. R. Zalupski, A. R. Cook and J. F. Wishart, The chemistry of separations ligand degradation by organic radical cations, *Proc. Chem.*, 2016, **21**, 61–65.
20 J. Drader, G. Saint-Louis, J. M. Muller, M.-C. Charbonnel, P. Guilbaud, L. Berthon, K. M. Roscioli-Johnson, C. A. Zarzana, C. Rae, G. S. Groenewold, B. J. Mincher, S. P. Mezyk, K. McCann, S. G. Boyes and J. Braley, Radiation chemistry of the branched-chain monoamide di-2-ethylhexylisobutyramide, *Solvent Extr. Ion Exch.*, 2017, **35**, 480–495.
21 G. P. Horne, C. A. Zarzana, T. S. Grimes, C. Rae, J. Ceder, S. P. Mezyk, B. J. Mincher, M.-C. Charbonnel, P. Guilbaud, G. Saint-Louis and L. Berthon, Effect of chemical environment on the radiation chemistry of N,N-di-(2-ethylhexyl)-butyramide (DEHBA) and plutonium retention, *Dalton Trans.*, 2019, **48**, 14450–14460.
22 B. J. Mincher and S. P. Mezyk, Radiation chemical effects on radiochemistry: A review of examples important to nuclear power, *Radiochim. Acta*, 2009, **97**, 519–534.
23 B. J. Mincher, G. Modolo and S. P. Mezyk, Review article: The effects of radiation chemistry on solvent extraction: 1. Conditions in acidic solution and a review of TBP radiolysis, *Solvent Extr. Ion Exch.*, 2009, **27**, 1–25.
24 B. J. Mincher, G. Modolo and S. P. Mezyk, Review article: The effects of radiation chemistry on solvent extraction: 2. A review of fission–product extraction, *Solvent Extr. Ion Exch.*, 2009, **27**, 331–353.
25 B. J. Mincher, G. Modolo and S. P. Mezyk, Review article: The effects of radiation chemistry on solvent extraction 3: A review of actinide and lanthanide extraction, *Solvent Extr. Ion Exch.*, 2009, **27**, 579–606.
26 B. J. Mincher, G. Modolo and S. P. Mezyk, Review article: The effects of radiation chemistry on solvent extractions 4: Separation of the trivalent actinides and considerations for radiation-resistant solvent systems, *Solvent Extr. Ion Exch.*, 2010, **28**, 415–436.
27 L. Berthon and M.-C. Charbonnel, Chapter 8 Radiolysis of solvents used in nuclear fuel reprocessing, in *Ion Exchange and Solvent Extraction: A Series of Advances*, ed. B. A. Moyer, 2009, vol. 19, pp. 429–514.
28 R. Malmbeck and N. L. Banik, Radiolytic behavior of a TODGA based solvent under alpha irradiation, *J. Radioanal. Nucl. Chem.*, 2020, **326**, 1609–1615.
29 H. Galan, C. A. Zarzana, A. Wilden, H. Nunez, R. J. M. Schmidt, A. Egberink, J. Leoncini, W. Cobos, G. Verboom, G. Modolo, S. Groenewold and B. J. Mincher, Gamma-radiolytic stability of new methylated TODGA derivatives for minor actinide recycling, *Dalton Trans.*, 2015, **44**, 18049–18056.
30 V. Hubscher-Bruder, V. Mogilireddy, S. Michel, A. Leoncini, J. Huskens, W. Verboom, H. Galan, A. Nunez, J. Cobos, G. Modolo, A. Wilden, H. Schmidt, M.-C. Charbonnel, P. Guilbaud and N. Boubals, Behaviour of the extractant Me-TODGA upon gamma irradiation: Quantification of degradation compounds and individual influences on complexation and extraction, *New J. Chem.*, 2017, **41**, 13700–13711.
31 H. Galan, A. Nunez, A. G. Espartero, R. Sedano, A. Durana and J. d. Mendoza, Radiolytic stability of TODGA: Characterization of degraded samples under different experimental conditions, *Proc. Chem.*, 2012, **7**, 195–201.
32 K. M. Roscioli-Johnson, C. A. Zarzana, G. S. Groenewold, B. J. Mincher, A. Wilden, H. Schmidt, G. Modolo and B. Santiago-Schübel, A study of the radiolysis of N, N-Didodecyl-N′,N′-Dioctyldiglycolamide using UHPLC-ESI-MS analysis, *Solvent Extr. Ion Exch.*, 2016, **34**, 439–453.
33 I. Sánchez-García, H. Galán, J. M. Perlado and J. Cobos, Stability studies of GANEX system under different irradiation conditions, *EPJ Nucl. Sci. Technol.*, 2019, **5**, 19–26.
34 I. Sanchez-Garcia, H. Galan, J. M. Perlado and J. Cobos, Development of experimental irradiation strategies to

evaluate the robustness of TODGA and water-soluble BTP extraction systems for advanced nuclear fuel recycling, *Radiat. Phys. Chem.*, 2020, **177**, 109094.

35 Y. Wang, Y. Wan, Y. Cai, L. Yuan, W. Feng and N. Liu, A review of the alpha radiolysis of extractants for actinide lanthanide separation in spent nuclear fuel reprocessing, *Radiochim. Acta*, 2021, **109**, 603–623.

36 Y. Sugo, M. Taguchi, Y. Sasaki, K. Hirota and T. Kimura, Radiolysis study of actinide complexing agent by irradiation with helium ion beam, *Radiat. Phys. Chem.*, 2009, **78**, 1140–1144.

37 Y. Sugo, Y. Sasaki, M. Taguchi and N. S. Ishioka, α-Radiation effect on solvent extraction of minor actinide, *J. Radioanal. Nucl. Chem.*, 2015, **303**, 1381–1384.

38 G. P. Horne, C. Celis-Barros, J. K. Conrad, T. S. Grimes, J. R. McLachlan, B. M. Rotermund, A. R. Cook and S. P. Mezyk, Impact of lanthanide ion complexation and temperature on the chemical reactivity of N,N,N′,N′-tetraoctyl diglycolamide (TODGA) with the dodecane radical cation, *Phys. Chem. Chem. Phys.*, 2023, **25**, 16404.

39 C. A. Zarzana, D. R. Peterman, G. S. Groenewold, L. G. Olson, R. G. McDowell, W. F. Bauer and S. J. Morgan, Investigation of the Impacts of Gamma Radiolysis on an Advanced TALSPEAK Separation, *Sep. Sci. Technol.*, 2015, **50**, 2836–2843.

40 D. R. Peterman, C. A. Zarzana, R. Tillotson, R. McDowell, C. Rae, G. S. Groenewold and J. Law, Evaluation of the impacts of gamma radiolysis on an ALSEP process solvent, *J. Radioanal. Nucl. Chem.*, 2018, **316**, 855–860.

41 S. N. Bhattacharyya and K. P. Kundu, The radiation chemistry of aqueous solutions of ferric ethylenediamine tetraacetate, *Int. J. Radiat. Phys. Chem.*, 1971, **3**, 1–10.

42 K. P. Kundu and N. Matuura, Gamma-radiolysis of ferric ethylene diamine tetra-acetate in neutral aqueous solution, *Int. J. Radiat. Phys. Chem.*, 1975, **7**, 565–571.

43 Y. A. Ilan and G. Czapski, The reaction of superoxide radical with iron complexes of EDTA studied by pulse radiolysis, *Biochim. Biophys. Acta*, 1977, **498**, 386–394.

44 B. K. Sharma and R. Gupta, γ-Radiolysis of aqueous solutions of cerium(III)-ethylenediamine tetraacetate, *Radiat. Eff. Lett. Sect.*, 1980, **57**, 149–154.

45 B. K. Sharma and R. Gupta, On the γ-radiolysis of aqueous solution of cerium(III) nitriloltriacetate, *Radiat. Phys. Chem.*, 1984, **24**, 233–237.

46 M. M. Khater, I. M. Kenawi, A. M. Atwa and M. B. Hafez, Radiolysis of NTA complexes with uranium(VI), iron(III) and nickel(II), *J. Radioanal. Nucl. Chem.*, 1987, **111**, 17–26.

47 M. B. Hafez, H. Roushdy and N. Hafez, Radiolysis of aqueous solutions of ethylenediaminetetraacetatocerium (III), *J. Radioanal. Chem.*, 1978, **43**, 121–129.

48 A. Kimberlin, G. Saint-Louis, D. Guillaumont, B. Cames, P. Guilbad and L. Berthon, Effect of metal complexation on diglycolamide radiolysis: a comparison between ex situ gamma and in situ alpha irradiation, *Phys. Chem. Chem. Phys.*, 2022, **24**, 9213–9228.

49 P. R. Zalupski, T. S. Grimes, C. R. Heathman and D. R. Peterman, Optical absorption characteristics for $^{7}F0' \rightarrow {}^{5}L6'$ and $^{7}F0' \rightarrow {}^{7}F6'$ transitions of trivalent americium ion in aqueous electrolyte mixtures, *Appl. Spectrosc.*, 2017, **7**, 2608–2615.

50 J. F. Wishart, A. R. Cook and J. R. Miller, The LEAF picosecond pulse radiolysis facility at Brookhaven National Laboratory, *Rev. Sci. Instrum.*, 2004, **75**(11), 4359–4366.

51 G. V. Buxton and C. R. Stuart, Re-evaluation of the thiocyanate dosimeter for pulse radiolysis, *J. Chem. Soc., Faraday Trans.*, 1995, **92**, 279–281.

52 B. J. Gullekson, M. A. Brown, A. Paulenova and A. V. Gelis, Speciation of Select F-Elements with Lipophilic Phosphorus Acids and Diglycol Amides in the ALSEP Backward-Extraction Regime, *Ind. Eng. Chem. Res.*, 2017, **56**(42), 12174–12183.

53 H. Fricke and E. J. Hart, The Oxidation of Fe^{++} to Fe^{+++} by the irradiation with X-rays of solutions of ferrous sulfate in sulfuric acid, *J. Chem. Phys.*, 1935, **3**, 60–61.

54 N. Kaltsoyannis and P. Scott, *The f elements*, Oxford University Press, 2007.

55 A. Kimberlin and K. L. Nash, Dimerization of 2-ethylhexylphosphonic acid mono-2-ethylhexyl ester (HEH[EHP]) as determined by NMR spectrometry, *Solvent Extr. Ion Exch.*, 2021, **39**, 38–55.

56 ADF 2020 SCM, ADF 2020, *Theoretical Chemistry*, Vrije Universiteit, Amsterdam, The Netherlands, 2020, **https://www.scm.com**.

57 G. te Velde, F. M. Bickelhaupt, E. J. Baerends, C. Fonseca Guerra, S. J. A. van Gisbergen, J. G. Snijders and T. Ziegler, Chemistry with ADF, *J. Comput. Chem.*, 2001, **22**, 931–967.

58 R. Bader, *Atoms in Molecules*, Oxford University Press, Oxford, 1990.

59 A. Becke, *The Quantum Theory of Atoms in Molecules: From Solid State to DNA and Drug Design*, John Wiley & Sons Inc., 2007.

60 F. Neese, The ORCA Program System, *Wiley Interdiscip. Rev.: Comput. Mol. Sci.*, 2012, **2**, 73–78.

61 F. Neese, Software Update: The ORCA Program System, Version 4.0, *Wiley Interdiscip. Rev.: Comput. Mol. Sci.*, 2018, **8**, e1327.

62 AIMAll and T. A. Keith, *AIMAll (Version 17.01.25)*, TK Gristmill Software, Overland Park KS, 2017.

63 A. Kerridge, Oxidation State and Covalency in F-Element Metallocenes (M = Ce, Th, Pu): A Combined CASSCF and Topological Study, *Dalton Trans.*, 2013, **42**, 16428.

64 M. J. Frisch, G. W. Trucks, H. B. Schlegel, G. E. Scuseria, M. A. Robb, J. R. Cheeseman, G. Scalmani, V. Barone, G. A. Petersson, H. Nakatsuji, X. Li, M. Caricato, A. V. Marenich, J. Bloino, B. G. Janesko, R. Gomperts, B. Mennucci, H. P. Hratchian, J. V. Ortiz, A. F. Izmaylov, J. L. Sonnenberg, D. Williams-Young, F. Ding, F. Lipparini, F. Egidi, J. Goings, B. Peng, A. Petrone, T. Henderson, D. Ranasinghe, V. G. Zakrzewski, J. Gao, N. Rega, G. Zheng, W. Liang, M. Hada, M. Ehara, K. Toyota, R. Fukuda, J. Hasegawa, M. Ishida, T. Nakajima, Y. Honda, O. Kitao,

H. Nakai, T. Vreven, K. Throssell, J. A. Montgomery Jr., J. E. Peralta, F. Ogliaro, M. J. Bearpark, J. J. Heyd, E. N. Brothers, K. N. Kudin, V. N. Staroverov, T. A. Keith, R. Kobayashi, J. Normand, K. Raghavachari, A. P. Rendell, J. C. Burant, S. S. Iyengar, J. Tomasi, M. Cossi, J. M. Millam, M. Klene, C. Adamo, R. Cammi, J. W. Ochterski, R. L. Martin, K. Morokuma, O. Farkas, J. B. Foresman and D. J. Fox, *Gaussian 16, Revision B.01*, Gaussian, Inc., Wallingford CT, 2016.

65 R. Dennington, T. A. Keith and J. M. Millam, *GaussView, Version 6.1.1*, Semichem Inc., Shawnee Mission, KS, 2016.

66 C. P. Kelly, C. J. Cramer and D. G. Truhlar, Aqueous solvation free energies of ions and ion–water clusters based on an accurate value for the absolute aqueous solvation free energy of the proton, *J. Phys. Chem. B*, 2006, **110**, 16066–16081.

67 C. P. Kelly, C. J. Cramer and D. G. Truhlar, Single-ion solvation free energies and the normal hydrogen electrode potential in methanol, acetonitrile, and dimethyl sulfoxide, *J. Phys. Chem. B*, 2007, **111**, 408–422.

68 B. J. Mincher, S. P. Mezyk, G. Elias, G. S. Groenewold, C. L. Riddle and L. G. Olson, The radiation chemistry of CMPO: Part 1. Gamma Radiolysis, *Solvent Extr. Ion Exch.*, 2013, **31**, 715–730.

69 G. Elias, G. S. Groenewold, B. J. Mincher and S. P. Mezyk, Determination of CMPO using HPLC-UV, *J. Chromatogr. A*, 2012, **1243**, 47–52.

70 B. J. Mincher, S. P. Mezyk, G. Elias, G. S. Groenewold, J. A. LaVerne, M. Nilsson, J. Pearson, N. C. Schmitt, R. D. Tillotson and L. G. Olson, The radiation chemistry of CMPO: Part 2. Alpha Radiolysis, *Solvent Extr. Ion Exch.*, 2014, **32**, 167–178.

71 B. J. Mincher and R. D. Curry, Considerations for choice of a kinetic figure of merit in process radiation chemistry for waste treatment, *Appl. Radiat. Isot.*, 2000, **52**, 189–193.

72 G. P. Horne, C. A. Zarzana, C. Rae, A. R. Cook, S. P. Mezyk, P. R. Zalupski, A. Wilden and B. J. Mincher, Does Addition of 1-Octanol as a Phase Modifier Provide Radical Scavenging Radioprotection for N,N,N′,N′-tetraoctyldiglycolamide (TODGA)?, *Phys. Chem. Chem. Phys.*, 2020, **22**, 24978–24985.

73 G. P. Horne, J. J. Kiddle, C. A. Zarzana, C. Rae, J. R. Peller, A. R. Cook, S. P. Mezyk and B. J. Mincher, ^{31}P NMR Study of the Activated Radioprotection Mechanism of Octylphenyl-N,N-diisobutyl-carbamoylmethyl Phosphine Oxide (CMPO) and Analogues, *Dalton Trans.*, 2019, **48**, 11547–11555.

74 L. Wojnarovits, Photochemistry and radiation chemistry of liquid alkanes: Formation and decay of low-energy excited states, in *Charged Particles and Photon Interactions with Matter: Chemical, Physicochemical, and Biological Consequences with Applications*, ed. A. Mozumder and Y. Hatano, CRC Press, Boca Raton, 2003.

75 G. P. Horne, T. S. Grimes, P. R. Zalupski, D. S. Meeker, T. E. Albrecht-Schonzart, A. R. Cook and S. P. Mezyk, Curium(III) radiation induced reaction kinetics in aqueous media, *Dalton Trans.*, 2021, **50**, 10853–10859.

76 S. P. Mezyk, G. P. Horne, B. J. Mincher, P. R. Zalupski, A. R. Cook and J. F. Wishart, The Chemistry of Separations Ligand Degradation by Organic Radical Cations, in *5th International ATALANTE Conference on Nuclear Chemistry for Sustainable Fuel Cycles. Procedia Chem.*, 2016, vol. 21, pp. 61–65.

77 J. H. Espenson, *Chemical Kinetics and Reaction Mechanisms*, McGraw-Hill, NY, 2nd edn, 1995, pp. 200–202. ISBN: 0-07-288362-6.

78 A. L. van Geet and A. W. Adamson, Diffusion in liquid hydrocarbon mixtures, *J. Phys. Chem.*, 1964, **68**, 238–246.

79 *Spartan 14v112*, Wavefunction, Inc., Irvine, 2013.

80 D. B. Dreisinger and W. C. Cooper, The diffusion coefficient of HEHEHP in heptane measured by the modified Stokes Cell technique at temperatures between 25 and 55 °C, *Solvent Extr. Ion Exch.*, 1990, **8**, 893–905.

81 G. R. Choppin and E. N. Rizkalla, Chapter 128 Solution chemistry of actinides and lanthanides, in *Handbook on the Physics and Chemistry of the Rare Earths*, ed. K. A. Gschneidner Jr., L. Eyring and G. R. Choppin, Elsevier Science B.V, Amsterdam, 1994, pp. 559–590.

82 E. J. Watkinson, R. Ambrosi, D. Freis, P. Lajarge, J.-F. Vigier, D. Bouexiere, S. Nourry, R. Konings, T. Tinsley, M. Sarsfield, K. Stephenson and J. Najorka, Americium Oxide Surrogate Studies: Pursuing European Radioisotope Power Systems Fuel Form Development, in *2019 IEEE Aerospace Conference*, Big Sky, MT, USA, 2019, pp. 1–9.

83 T. S. Grimes, G. Tian, L. Rao and K. L. Nash, Optical Spectroscopy Study of Organic-Phase Lanthanide Complexes in the TALSPEAK Separations Process, *Inorg. Chem.*, 2012, **51**, 6299–6307.